JOURNAL OF GEOPHYSICAL RESEARCH, VOL. 106, NO. C8, PAGES 16,673–16,684, AUGUST 15, 2001

# Intense surface currents in the tropical Pacific during 1996–1998

Semyon A. Grodsky and James A. Carton

Department of Meteorology, University of Maryland, College Park, Maryland

**Abstract.** Tropical Pacific Ocean near-surface currents and their momentum and temperature balances are investigated using several data sets, including drifting buoy velocities and TOPEX/Poseidon altimetry. The data sets are combined to produce monthly surface current estimates on a uniform grid for the 6-year period 1993–1998, using multivariate optimal interpolation. The analysis shows dramatic changes in current from December 1996 through August 1998 in response to the recent El Niño–Southern Oscillation event. Eastward current anomalies of $\sim$1 m $s^{-1}$ were recorded in December 1996 in the western Pacific, generated by sporadic westerly wind bursts. By April 1997 these equatorial anomalies reached the eastern boundary, and in the summer of 1997 a band of strong eastward flow formed across the basin. This circulation pattern persisted until the beginning of 1998, when a westward equatorial jet appeared in January–April. Interestingly, the reversal of flow occurred prior to the restoration of the trade winds. The timing of these events as well as the results of previous dynamical studies raise questions about the relative importance of terms in the zonal momentum and temperature balances. We address the first of these questions by examining the applicability of a three-term linear zonal momentum balance on the equator. In all cases we focus on anomalies from the time mean. Our results show that local acceleration is reasonably well balanced by the difference between zonal pressure gradient anomaly and wind-induced momentum flux. This three-term balance displays significant basin-wide variations and is consistent with the conclusion that the equatorial Pacific is not in equilibrium with local wind forcing due to the presence of propagating waves. Examination of the temperature balance shows that at the beginning of El Niño the warming in the central Pacific is mainly supported by horizontal temperature transport, while the vertical heat exchange and transport become important in the eastern half of the equatorial Pacific during the transition from El Niño to La Niña.

## 1. Introduction

Although many models of air/sea interaction in the tropical Pacific assume that mixed layer temperature is controlled by diabatic mixing at its base [e.g., *Suarez and Schopf*, 1988], others assume that it is governed by the mass and heat dynamics in the western Pacific warm pool, with zonal transport playing a key role [see, e.g., *Wyrtki*, 1985]. Indeed, *Picaut et al*. [1996] found that much of the monthly shift in the position of the pool of warm surface water that normally resides in the western basin can be explained by zonal advection of water within the mixed layer. Picaut et al. also found that the boundary between the warm pool of water to the west and the cooler water to the east defines a region of zonal convergence and subduction. The potential role of such advective processes in controlling sea surface temperature (SST) complicates our understanding of the air/sea feedback cycles leading to El Niño–Southern Oscillation (ENSO) [*Picaut et al*., 1997; *An et al*., 1999; *Jin and An*, 1999]. The purpose of this paper is to reexamine the contribution of horizontal advection to momentum and heat balances in the tropical Pacific during the extreme events of 1997–1998, making use of the extensive surface drifter and sea level data sets now available.



Paper number 2000JC000481.
0148-0227/01/2000JC000481$09.00

There is strong independent experimental evidence [see, e.g., *Johnson and Luther*, 1994; *Qiao and Weisberg*, 1997] that the momentum balance on seasonal and interannual timescales is generally linear and geostrophic away from the equator. Along the equator, *Yu and McPhaden* [1999] examined Tropical Atmosphere-Ocean (TAO) buoy data at four mooring locations and found a three-term balance in the zonal momentum equation between local acceleration, pressure gradient force, and wind stress whose relative strength must change as wind intensity and direction shift.

Recently, a suite of studies has revisited the ocean's role in regulating SST on seasonal and interannual timescales [e.g., *Köberle and Philander*, 1994; *Picaut et al*., 1996; *Delcroix and Picaut*, 1998; *Moisan and Niiler*, 1998; *Kessler et al*., 1998; *DeWitt and Schneider*, 1999; *Swenson and Hansen*, 1999]; however, the conclusions have not been uniform. Modeling studies by *Köberle and Philander* [1994] and *DeWitt and Schneider* [1999] suggest that the annual cycle of SST in the eastern basin results from entrainment of cool subthermocline water into the mixed layer because of meridional divergence of surface waters, while *Swenson and Hansen* [1999] argue that local storage is also important. In contrast, *Kessler et al*. [1998] conclude that three-dimensional temperature advection terms tend to cancel each other and, to first order, the seasonal variation of SST can be described as simply following the variation of net surface heat flux. It is still debatable whether or not the same terms dom-

inate for interannual processes such as ENSO. Tropical instability waves [*Baturin and Niiler*, 1997] may also contribute to seasonal and interannual cycles because of their seasonality and dependence on mean shear.

In the central and western basin the story of the heat budget is complicated as well. As mentioned above, *Picaut et al*. [1996] and *Delcroix and Picaut* [1998] argue that on interannual timescales, changes of mixed layer temperature largely reflect changes in the anomalous zonal advection of water acting on the mean westward temperature gradient, while *Wang and McPhaden* [1999] additionally argue for the importance of surface heat flux.

The massive El Niño of 1997–1998 provides an exciting opportunity to reexamine the momentum and heat balances of the tropical Pacific under extreme conditions. The story of this El Niño begins with a series of westerly wind bursts in the western basin in late 1996 [*Yu and Rienecker*, 1998; *McPhaden*, 1999; *Wang and Weisberg*, 2000]. These westerly wind bursts, an enhancement of the normal Madden Julian Oscillation, were followed by a relaxation of the trade winds and warming of SST near the dateline in January–February 1997 and in the east by March. Instantaneous zonal velocity transects from acoustic Doppler current profiler (ADCP) meridional vertical sections taken from October 1996 through November 1998 by *Johnson et al*. [2000] show a strong eastward surface current anomaly on the equator in response to the relaxing trade winds, with peak velocities approaching 1 m $s^{-1}$. As warm conditions were rapidly replaced by cold La Niña conditions and the trade winds accelerated (see *McPhaden* [1999] for a discussion), the current anomalies also reversed direction, forming a westward jet with its maximum speed (>1 m $s^{-1}$) north of the equator. However, spatial discreteness and time sampling of these data complicate the assessment of time and spatial derivatives needed to estimate the momentum and heat budgets.

Fortunately for the cause of trying to understand momentum and heat balances during these extreme events, several new data sets have become available in recent years. Extensive deployments of drogued surface drifters by the World Ocean Circulation Experiment Surface Velocity Programme [*Niiler et al*., 1987; *Hansen and Poulain*, 1996] now provide ~3000–4000 buoy days of direct currents observations per month in the tropical Pacific [*Acero-Schertzer et al*., 1997]. Much of the tropical ocean is in near-geostrophic balance with surface pressure. Thus satellite-based altimetry from the joint U.S./French TOPEX/Poseidon mission provides a powerful additional constraint on near-surface velocity. Indeed, *Yu et al*. [1995] have shown that the velocity estimates from these two data sets are remarkably consistent. We believe that the difference between the two is due to (ageostrophic) wind-driven effects, which *Ralph and Niiler* [1999] show can be explained to a considerable degree by Ekman-like dynamics, except when close to the equator.

The velocity analysis that we use for this study was constructed by combining drifter velocity and sea level data using multivariate optimal interpolation [*Carton and Hackert*, 1989; *Daley*, 1991]. We estimate the background (first guess) current as the long-term mean of drifter velocities. This background field is corrected with monthly mean observational increments of altimeter sea level and drifter data. We separately estimate geostrophic and ageostrophic components of the total velocity. Geostrophic error covariances have been extended to the equatorial $\beta$ plane on the basis of the Kelvin wave scaling of *Picaut et al*. [1989] and *Menkes et al*. [1995]. A simple linear friction is included to allow an Ekman-like balance to account for the ageostrophic component on the equator, following *Lagerloef et al*. [1999]. Our presentation of results begins with a kinematic description of currents during 1996–1998 followed by a discussion of the corresponding zonal momentum and thermal balances.

## 2. Data and Analysis

This study is based on four data sets: altimeter sea level, drifter velocity, SST, and National Center for Environmental Prediction (NCEP) wind stress and surface heat fluxes. The TOPEX/Poseidon altimeter sea level is obtained from the Pathfinder version 2.1 archive [*Koblinsky et al*., 1997]. These data are available with a 9.92-day repeat cycle spanning the period from late September 1992 through November 1998. After the usual corrections for geophysical effects the sea level estimates have been averaged into 1° latitude segments. The nominal accuracy of these estimates when averaged monthly is 2 cm [*Cheney et al*., 1994], while observed sea level anomalies are at least 4 times that amount.

The drouged surface drifter currents are obtained from the World Ocean Circulation Experiment/Tropical Ocean–Global Atmosphere archive at the Atlantic Ocean Marine Laboratory/National Oceanic and Atmospheric Administration (NOAA). The data span the period from 1979 to November 1998. After the processing described by *Hansen and Poulain* [1996] we averaged currents into 3° longitude × 2° latitude × 1 month bins. These data form the basic velocity data set for this study. For velocity comparisons, additional moored velocity time series were obtained from the Pacific Marine Environmental Laboratory/NOAA [*McPhaden et al*., 1998]. An additional experiment was conducted including these moored observations in order to improve our estimates of currents along the equator.

The surface wind stress and the net heat flux through the ocean surface are obtained from monthly mean NCEP/National Center for Atmospheric Research reanalysis product [*Kalnay et al*., 1996]. SST is the combined satellite advanced very high resolution radiometer (AVHRR)/in situ analysis of *Reynolds and Smith* [1994]. For the purpose of this study the wind stress, the heat flux, and the SST fields have been averaged into 3° × 2° × 1 month bins.

Our analysis methodology is a form of multivariate optimal interpolation [see *Daley*, 1991], which is briefly summarized here. Let $\mathbf{r}_k$, $1 \le k \le K$, define the analysis grid, while the spatial vectors $\mathbf{r}_m$, $1 \le m \le M$, and $\mathbf{r}_n$, $1 \le n \le N$, are the observation station locations for sea level $\eta$ and mixed layer velocity $\mathbf{u}$, respectively. The analysis velocity $\mathbf{u}^A$ may be written as a linear combination of the weighted differences between observations and a background estimate of sea level and velocity vector:

$$\mathbf{u}_k^A = \mathbf{u}_k^B + W_{km}^{U\eta}(\eta_m^O - \eta_m^B) + W_{kn}^{\mathrm{UU}}(\mathbf{u}_n^O - \mathbf{u}_n^B). \qquad (1)$$

There are several possible choices for use as the background velocity field $\mathbf{u}_k^B$, $\mathbf{u}_n^B$. *Lagerloef et al*. [1999] derive flow estimates using a background estimate based on spatially smoothed altimetry, hydrographic climatology, and wind drift. A disadvantage of this approach is the introduction of bias into the background error. Here we have explored the use of the long-term average surface drifter field to define $\mathbf{u}_k^B$, $\mathbf{u}_n^B$. The background estimate of sea level, $\eta^B$, is similarly derived from

the long-term averaged altimeter data. Sea level appears in (1) only in the form of observational increment, $\eta^O - \eta^B$.

Much of the challenge in applying (1) is in evaluating the weights, **W**. We do this by minimizing the analysis error variance in (1), assuming unbiased, stationary statistics [see *Daley*, 1991]:

$$\mathbf{W} = \mathbf{C} \cdot (\mathbf{B} + \mathbf{O})^{-1}, \tag{2}$$

where $\mathbf{C} = [\mathbf{C}^{U\eta}, \mathbf{C}^{UU}]$ is the $K(M + 2N)$ matrix of covariances between background velocity and sea level error components evaluated at the analysis and observation station locations. Similarly, **B** and **O** are $(M + 2N)(M + 2N)$ matrices containing background and observation error covariances evaluated at different station locations:

$$\mathbf{B} = \begin{bmatrix} \mathbf{B}^{\eta\eta} & \mathbf{B}^{\eta U} \\ \mathbf{B}^{U\eta} & \mathbf{B}^{UU} \end{bmatrix}, \qquad \mathbf{O} = \begin{bmatrix} \mathbf{O}^{\eta\eta} & \\ & \mathbf{O}^{UU} \end{bmatrix}. \tag{3}$$

Thus the weights **W** are small if the observations are either inaccurate or so closely distributed that they are duplicative. The elements of **C**, **B**, and **O** are difficult to estimate accurately. Instead of trying to do this we apply a variety of simplifying assumptions. First, we assume that **O** is diagonal, meaning that the observation errors are uncorrelated. Normalizing **O** by the analysis variance (assumed homogeneous), the elements along the diagonal of **O** are simply the ratio of noise-to-signal variances. This ratio we assume to be 4 for 1-s averaged altimetry, following *Carton et al*. [1996]. We do not yet have good estimates of the noise-to-signal ratio for velocity observations because of our lack of knowledge of unresolved physical processes. Here we assume a ratio of 0.2, following *Carton and Hackert* [1989]. Finally, we set the background error covariance noise-to-signal ratios to 1. Observational noise is a combination of instrument error and error of interpolation including that introduced by unresolved physics. One problem in particular is noise due to aliasing of inertial motions and tropical instability waves into the drifter observations. We attempt to mitigate these effects by only including measurements at locations where at least 10 buoy days/month of independent observations are available.

To complete our statistics, we begin by defining the background sea level error covariance $\mathbf{B}^{\eta\eta}$ and deriving all other background error covariances from this. To assure that all derived error covariances have appropriate properties (i.e., positive definiteness, compactness, and continuous derivatives), we choose $\mathbf{B}^{\eta\eta}$ to have a very simple homogeneous Gaussian form:

$$\mathbf{B}^{\eta\eta}(\mathbf{r}_p, \mathbf{r}_q) = \mathrm{Cov}\,(\eta_p, \eta_q) = (\sigma^\eta)^2 \exp\left[-\frac{\Delta x^2}{r_x^2} - \frac{\Delta y^2}{r_y^2}\right],$$

$$r_x = 450 \text{ km}, \quad r_y = 250 \text{ km}, \tag{4}$$

where $(\sigma^\eta)^2$ is the sea level error variance, assumed to be spatially homogeneous, and where $(\Delta x, \Delta y)$ are the zonal and meridional displacements of the vector $\Delta\mathbf{r} = \mathbf{r}_q - \mathbf{r}_p$. Our estimates of horizontal length scales, $r_x$, $r_y$, follow those of *Carton et al*. [2000].

In order to derive the remaining covariance submatrices it is helpful and reasonable to assume a dynamical relationship between sea level and velocity. We begin by assuming that analysis, observation, and background velocity can be decomposed into a geostrophic and a wind-driven component, $\mathbf{u} = \mathbf{u}_g + \mathbf{u}_w$. Following *Lagerloef et al*. [1999], we assume that $\mathbf{u}_w$ satisfies an Ekman-like equation balancing the difference between wind-induced momentum flux $\tau$ and linear friction by the Coriolis force:

$$f\mathbf{k} \times \mathbf{u}_w = \frac{\tau}{\rho H} - \frac{r\mathbf{u}_w}{H}, \tag{5}$$

where **k** is the vertical unit vector and $\rho$ is water density. Some assumption must be made regarding $H$, the depth scale over which wind-induced momentum is distributed (see *Ralph and Niiler* [1999] for discussion of possible options). Here we use the thickness of the ocean mixed layer provided by the ocean reanalysis of *Carton et al*. [2000] as a proxy for $H$ and estimate the friction coefficient $r$ by assuming that the mean meridional velocity near the equator is mainly wind-driven. On the basis of this assumption we estimate $r = 2 \times 10^{-4}$ m s$^{-1}$, a value similar to that proposed by *Lagerloef et al*. [1999]. Then we subtract $\mathbf{u}_w$ from each term ($\mathbf{u}_k^A$, $\mathbf{u}_n^O$, and $\mathbf{u}_n^B$) before evaluating (2). Thus (2) becomes an equation for the geostrophic component of $\mathbf{u}^A$. Evaluation of (2) requires error covariances. These are derived from (4) by applying geostrophy and are presented in Appendix A. The error variances and covariances vary spatially. We account for these variations by solving (1) in a series of $5 \times 3$ (longitude $\times$ latitude) grid point patches ($10° \times 9°$).

Within a radius of deformation of the equator the Coriolis term can no longer be considered constant within a grid patch, and indeed, the geostrophic approximation may be invalid. However, if we accept Kelvin wave scaling following *Menkes et al*. [1995], then we can assume that background errors (again these are differences between the first guess and the true value) for zonal geostrophic velocity $\delta u_g$ on the equator are related to background sea level errors $\delta\eta$ as $\delta u_g = -(g/\beta)\partial^2(\delta\eta)/\partial^2 y$. Following *Carton and Hackert* [1989] and *Lagerloef et al*. [1999] and allowing a smooth transition to equatorial dynamics,

$$\delta u_g = -F(\varphi)\,\frac{g}{f}\,\frac{\partial(\delta\eta)}{\partial y} - [1 - F(\varphi)]\,\frac{g}{\beta}\,\frac{\partial^2(\delta\eta)}{\partial y^2}, \tag{6}$$

$$\delta v_g = F(\varphi)\,\frac{g}{f}\,\frac{\partial(\delta\eta)}{\partial x},$$
$$F(\varphi) = 1 - \exp\,[-(\varphi/2.2°)^2], \tag{7}$$

where $F(\varphi)$ decreases smoothly as latitude $\varphi$ approaches zero with a scale estimated by the first-mode equatorial radius of deformation. The proper assumption to make for the meridional velocity component error $\delta v_g$ is less clear. Following the Kelvin wave analogy, we have assumed that background errors of sea level and meridional velocity decorrelate near the equator, as expressed in (7). For a positive sea level error on the equator, (6) and (7) together imply convergence to the east of the anomaly and divergence to the west.

The analysis results for March 1998 are illustrated in Figure 1. This analysis takes place during the late stage of the intense 1997–1998 El Niño when equatorial currents are already westward at speeds of up to 1 m s$^{-1}$ in the west. In the east the currents are weaker, indicating divergence in the zonal direction. North of the equator a weak eastward countercurrent is evident in the analysis even though it is not apparent in the drifter observations. The drifter data coverage during this month is not dense along the equator because of the dispersing effects of the strong currents.

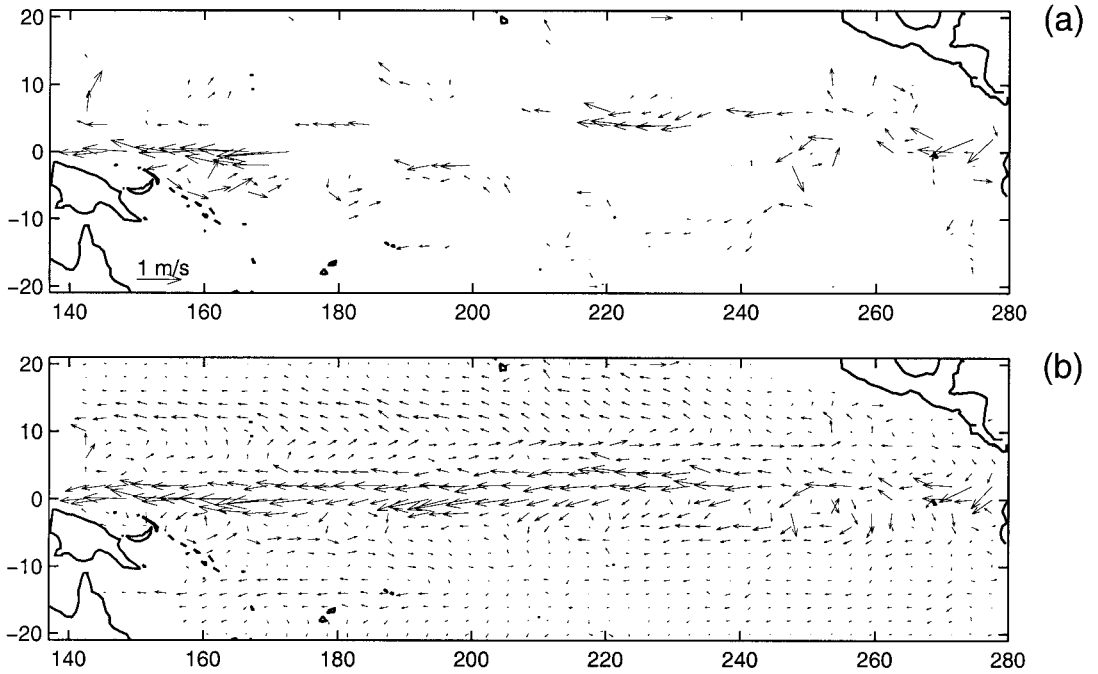


**Figure 1.** Velocity for March 1998. (a) Drifter velocity observations and (b) analysis velocity.

The relative impact of sea level and drifter observations as well as the accuracy of the analysis are explored in Figure 2. At three equatorial locations (165°E, 140°W, and 110°W) the mean analysis (and observed) zonal velocities were 22 cm $s^{-1}$ (10 cm $s^{-1}$), −15 cm $s^{-1}$ (−19 cm $s^{-1}$), and −19 cm $s^{-1}$ (−14 cm $s^{-1}$) based on the same time during which buoy data are available. Hence the difference between the buoy and the analysis currents does not exceed 25% of the standard deviation of current (around 50 cm $s^{-1}$ for zonal velocity). The largest bias of 12 cm $s^{-1}$ at 165°E may simply reflect statistical uncertainty (the buoy at this location was only in operation for 3.5 years). The mean analysis (and observed) meridional components were 0.5 cm $s^{-1}$ (1 cm $s^{-1}$), −3 cm $s^{-1}$ (−1 cm $s^{-1}$), and 2 cm $s^{-1}$ (5 cm $s^{-1}$). The differences are small compared to standard deviation of meridional current, which is around 10 cm $s^{-1}$. The standard deviations of analysis minus observed difference velocities are 29, 38, and 31 cm $s^{-1}$ for the zonal component and 16, 12, and 10 cm $s^{-1}$ for the meridional component at 165°E, 140°W, and 110°W, respectively. When the analysis is based solely on sea level ($\eta$) observations (the first two terms on the right-hand side of (1)), the main features of variability remain although the amplitudes are reduced.

## 3. Results

We begin our presentation of results by examining the changes in surface current during the dramatic events of 1997–1998. Throughout the following discussion the time mean 1993–1998 fields ($\bar{\mathbf{u}}$, $\bar{T}$, $\bar{\eta}$) are removed. This focuses attention on the behavior of anomalies from the time mean. We choose not to remove the seasonal cycle because of the close connection between seasonal cycle and ENSO. For the latest 1997–1998 ENSO event this connection was clearly demonstrated by *McPhaden* [1999].

In late 1996 a strong eastward current developed in the western Pacific basin in response to local westerly wind bursts (Figure 3). By March–April 1997 the ocean responded to these disturbances in wind and current with a simultaneous increase in SST and sea level in the central and eastern basins (see Figure 4, April 1997), while the eastward current became concentrated in the equatorial zone. During this season the strong eastward equatorial current was down the slope of sea level, while off the equator the current was weaker and variable. However, as 1997 progressed, the region of westerly wind anomalies shifted eastward and the equatorial current in the west weakened (December 1997 in Figure 4). For much of 1996 and early 1997, SST changed in phase with zonal velocity along the equator (see Figure 3). This, coupled with a negative zonal gradient of SST to the west along the equator, suggests an important role for advection in regulating central and eastern SST.

In midbasin the current remained eastward even though the pressure gradient reversed sign, so that by August the eastward current was flowing up the slope of sea level. Interestingly, east of 120°W a temporary reversal of eastward flow appeared in August–September 1997 (see Figure 3 and Figure 4, August) and was also observed in ADCP transports by *Johnson et al.* [2000]. The presence of a local westward jet in the eastern equatorial Pacific occurred in conjunction with the cooling of SST (compare zonal velocity and SST in Figure 3). The eastward equatorial current persisted until the boreal spring of 1998 when it shifted to westward west of 150°W, again allowing the current to flow downhill (see Figure 4, April 1998). By the fall of 1998 the zonal pressure gradient relaxed, although the current continued to flow westward. During this later stage, zonal advection and SST do not seem closely linked (see also Figure 5). The equatorial currents swung to the west between December and January, but SST remained high through April 1998. This suggests that advection plays a lesser role in regulating SST during this stage.

In this kinematic discussion it has been evident that changes

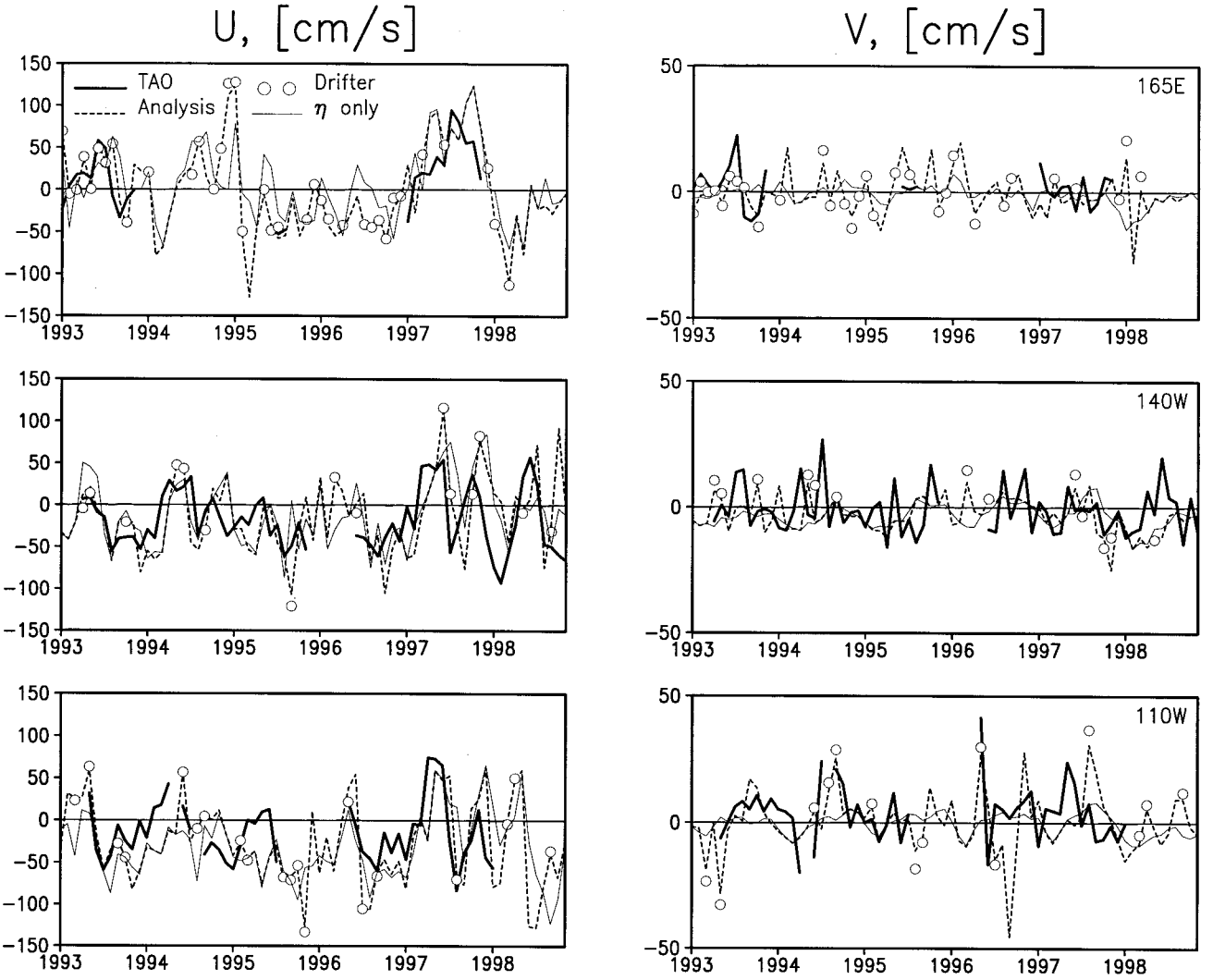


**Figure 2.** Velocity comparisons at three mooring locations. Four estimates are compared: 10-m moored currents (TAO), surface drifter observations (drifter), and analysis velocity (analysis), and analysis velocity without drifter data ($\eta$ only).

in the zonal pressure gradient follow shifts in the direction of the equatorial currents. The correspondence between variations of zonal velocity and SST varies significantly with time and becomes smaller during the late stage. To obtain a more quantitative understanding of the relationship between these terms, we now evaluate the zonal momentum balance and temperature budget.

There is strong experimental evidence to conclude [see, e.g., *Johnson and Luther*, 1994] that the momentum balance is linear and geostrophic to within 5° of the equator. *Qiao and Weisberg* [1997] extend this conclusion into the equatorial zone by showing that the momentum balance in the equatorial mixed layer remains essentially linear. This balance was also investigated at four TAO mooring locations by *Yu and McPhaden* [1999]. On seasonal cycle and interannual timescales they found a three-term balance between local acceleration $\partial u/\partial t$, zonal pressure gradient force $-g\partial\eta/\partial x$, and wind stress $\tau^x$:

$$\frac{\partial u}{\partial t} = -g\frac{\partial \eta}{\partial x} + \frac{\tau^x}{\rho H}. \tag{8}$$

At interannual timescales, acceleration is small, and the pressure gradient force balances wind stress. Zonal currents are in phase with these two terms, as was explicitly shown by *Johnston and Merrifield* [2000], who found that interannual geostrophic current anomalies derived from the tide gauge network data vary in phase with both zonal wind stress and sea level in the near-equatorial western Pacific Ocean. At shorter seasonal periods, acceleration becomes important, so that the development of an anomalous zonal pressure gradient lags behind changes in wind stress and local acceleration. Although the mooring data provide good sampling in time and depth, their spatial coverage is very limited. Here we apply methodology similar to that of *Johnston and Merrifield* [2000] to examine the applicability of this three-term balance throughout the basin during the extreme events of 1997–1998.

Figure 6 shows results for 3 months during the early, middle, and late stages of El Niño. For this comparison, acceleration and spatial derivatives have been estimated using central differences. Error estimates (see Appendix B) are included in

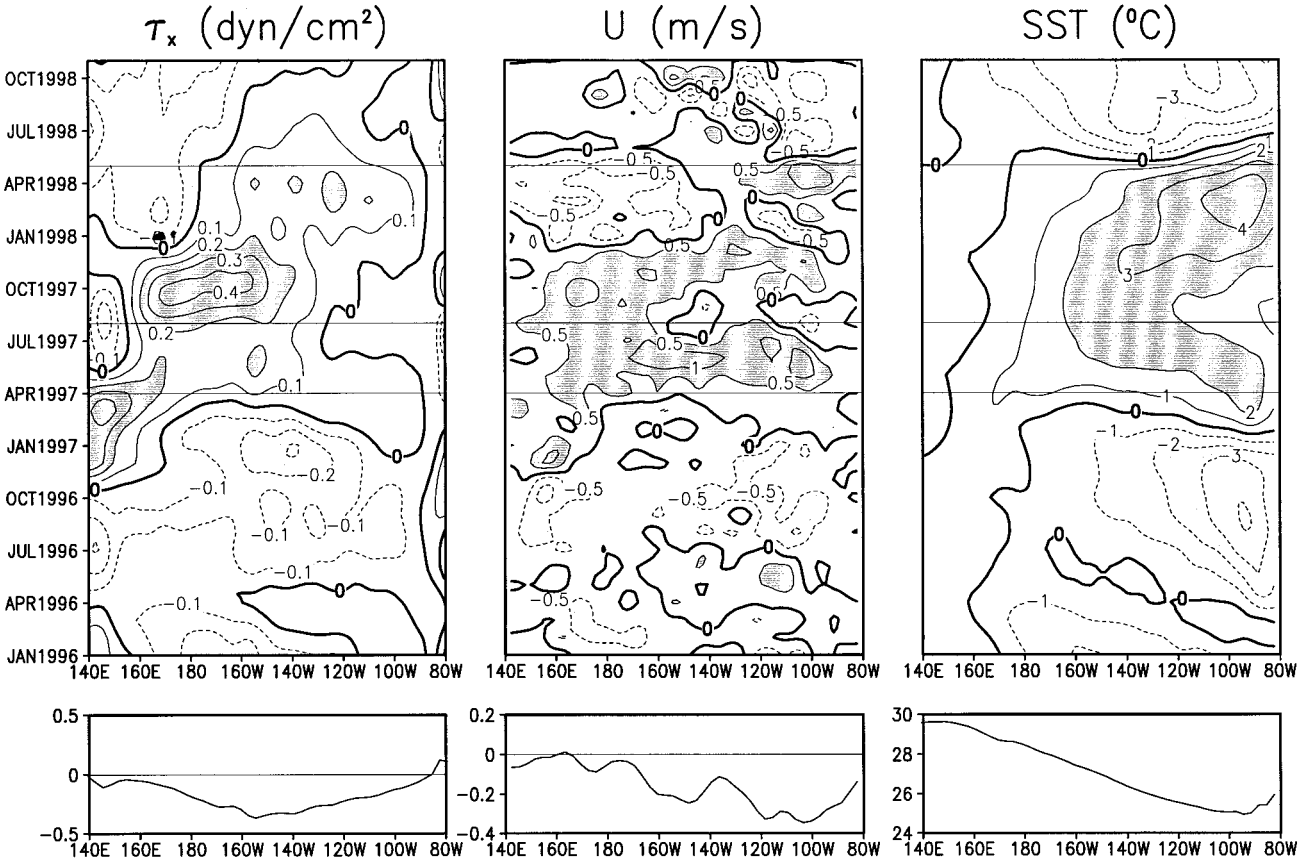


**Figure 3.** (top) Time-longitude equatorial cross section of (left) zonal wind stress, (middle) surface velocity, and (right) SST during 1996–1998. (bottom) Time average removed from each field. Horizontal lines mark the times for which the estimates of the upper ocean momentum and temperature balances are shown in Figures 6 and 8.

Figure 6 (bottom) to indicate the uncertainties in the various data sets. We select April 1997 to represent the early stage of El Niño, when the currents reverse and SST is increasing (see Figure 3). We choose August 1997 to characterize the conditions during the middle stage, when the rate of change of the SST is relatively low. We choose May 1998 to represent the late stage, when the SST begins to drop in the eastern basin.

In April 1997, when the easterly winds begin to reverse, they can no longer balance the negative pressure gradient associated with sea level. As a result, the currents across the basin accelerate eastward. The close balance between the three terms in (8) suggests, to within the errors of estimates, that friction and nonlinearity play lesser roles during this onset phase in the surface layer. Including our estimates of horizontal advection, for example, does not improve agreement between acceleration and force terms in (8); however, our estimate is quite uncertain ($\pm 5 \times 10^{-7}$ m s$^{-2}$).

By the middle stage (August 1997) the positive trade wind anomalies have extended farther eastward nearly in balance with the pressure gradient force. As a result, the zonal acceleration is close to zero along the equator west of 150°W. For 50° east of 150°W an eastward pressure gradient accelerates a westward current (see Figure 3 and 140°W and 110°W in Figure 2). By the late stage (May 1998) the positive trade wind anomalies have shifted far to the east. However, an intense negative pressure gradient force causes a strong westward acceleration of up to 4 cm s$^{-1}$ d$^{-1}$. In summary (see Figure 7), the three-term balance applies for much of the basin (correlation >0.4). The exception is a 20° band of longitudes from 140°W to 120°W. In this band of longitudes, which is a region of rather strong zonal gradient of the thermocline depth and cool surface temperatures, acceleration and the sum of wind stress and pressure gradient force become uncorrelated. The low correlation is not a result of missing advection or of near-equatorial sampling problems. It is not improved by including observations from the TAO moorings in the analysis. We believe that the missing dynamics are nonlinearity (at least, vertical advection) and mixing processes. We can anticipate similar results for the heat budget.

Now we examine the heat balance during the same three stages examined for momentum, focusing on spatial variations along the equator. Written for anomalies from the long-term mean and averaged over the upper ocean mixed layer of depth $H$, this balance becomes, following *Moisan and Niiler* [1998],

$$\frac{\partial T}{\partial t} = -[\mathbf{u} \cdot \nabla \bar{T} + \bar{\mathbf{u}} \cdot \nabla T + \mathbf{u} \cdot \nabla T] + \frac{(F_0 - F_w)}{C_p \rho H}, \quad (9)$$

where $C_p$ is specific heat capacity of water and $F_0$ and $F_w$ are downward anomaly heat fluxes across the air-sea interface and at the bottom of the mixed layer, respectively. $F_0$ represents the net surface radiative flux actually absorbed by the mixed layer (following *Wang and McPhaden* [1999]), and $F_w$ represents the heat flux out of base of the mixed layer and is a combination of entrainment and vertical turbulent diffusion.

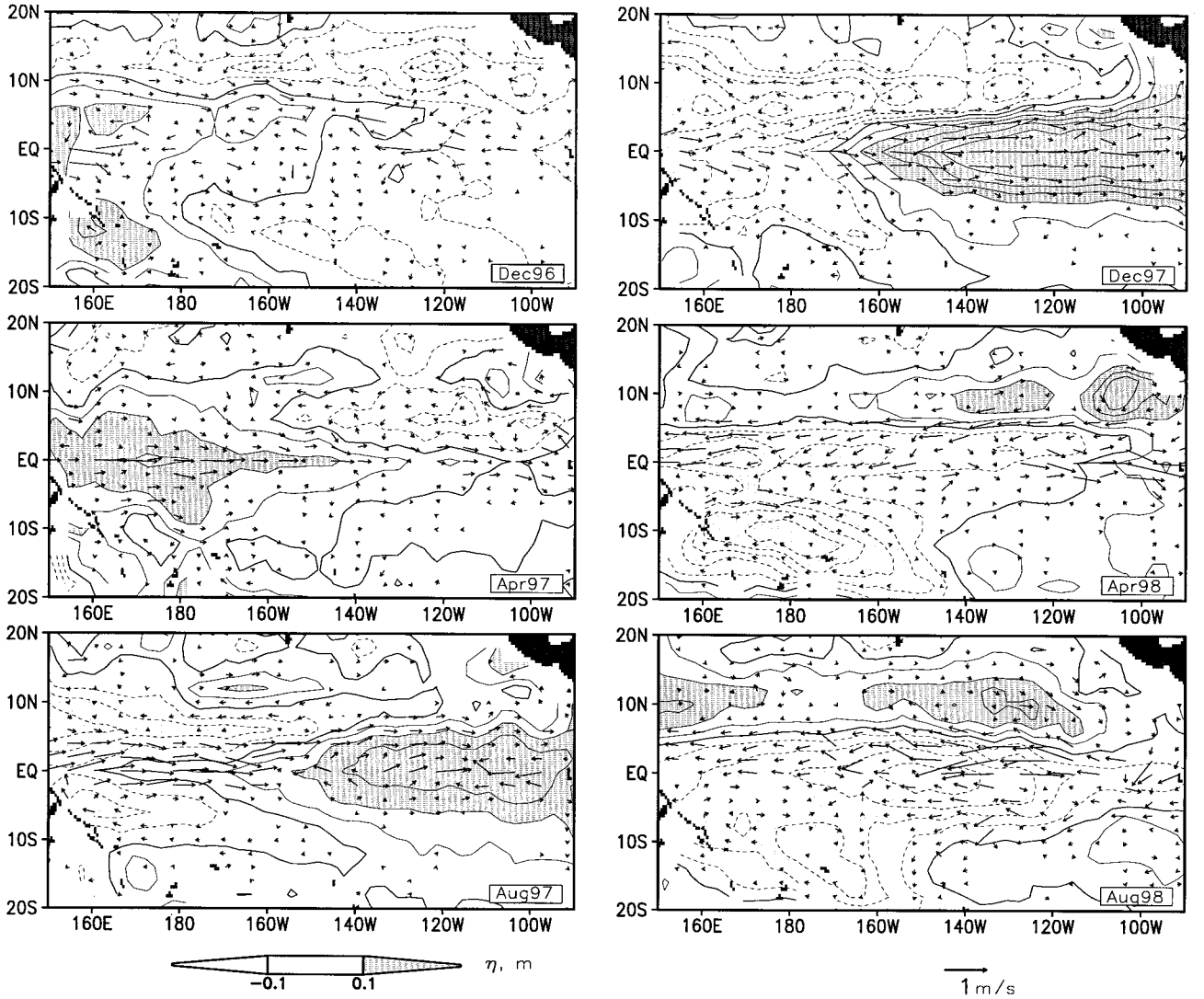


**Figure 4.** Monthly sea level anomalies (shading) and velocity anomalies (arrows) from the climatological mean for every 4 months from December 1996 through August 1998. Contour interval is 5 cm. Only sea level anomalies exceeding 10 cm are shaded. Only currents greater than 10 cm $s^{-1}$ are shown.

We estimate all terms in (9), except $F_w$, using velocity analysis, SST, surface fluxes, and mixed layer depth. Then we diagnose times/places where $F_w$ might be significant by comparing the SST rate of change to the sum of terms on the right-hand side of (9), accounting for the effects of horizontal transport and surface fluxes. For this comparison, rate of change and spatial derivatives were estimated as central differences.

During the early stage (see Figure 8, April 1997), accelerating eastward currents transport the waters of the western warm pool toward the east. This transport is mainly due to anomaly current advection acting on the mean SST gradient $-(\mathbf{u} \cdot \nabla \bar{T})$, and gives warming east of 180°W. Net surface flux is small except east of 120°W, where it acts to cool the ocean. This drop results from two factors: first, a drop in incoming short-wave radiation resulting from increased cloudiness over already warm waters and second, an increase of latent heat loss. Surface flux, advection, and heat storage rate balance west of 110°W to within our error estimates. Thus heat flux due to other processes such as entrainment must play a lesser role. We conclude that during this early stage the increase of SST is balanced by eastward advection of warm pool waters by the zonal current, as was suggested by *Picaut et al.* [1996] and *Delcroix and Picaut* [1998]. East of 110°W the left- and right-hand sides of (9) balance each other to within the errors of our data. Nevertheless, $\partial T/\partial t$ exceeds the sum of fluxes. Examination of the ocean reanalysis shows that the mixed layer thickness averaged 120°–80°W increased to 30–35 m from the 15–20 m observed in late 1996. This deepening of the thermocline acts to reduce the effect of heat loss across the bottom of the mixed layer on its temperature because of larger $H$.

During the middle stage (see Figure 8, August), SST is relatively steady ($\partial T/\partial t \approx 0$). Heat gain by horizontal advection is compensated for by surface heat loss over already warm waters west of 120°W. East of 120°W, surface heat loss increases while horizontal advection remains small, and additional heat gain to the mixed layer is needed to complete the balance. Examination of the ocean reanalysis shows that the mixed layer depth (120°W–80°W) increases by 25 m, again acting to reduce the effect of heat loss across its bottom on the SST. Note that our reasoning regarding the need for the anom-

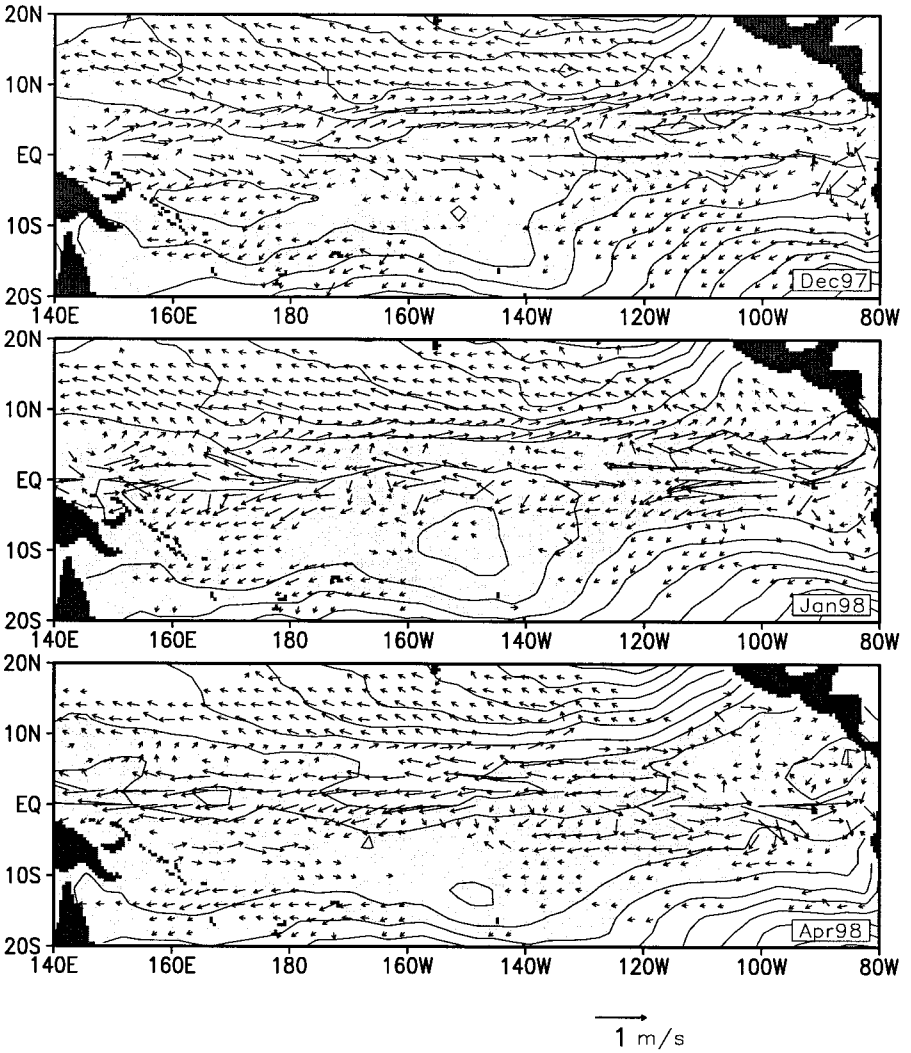


**Figure 5.** Monthly mean currents (arrows) and SST (shading) from December 1997 through April 1998. Contour interval is 1°C. Only areas with SST exceeding 28°C are shaded. Only currents greater than 10 cm $s^{-1}$ are shown.

aly heat gain into the deepening mixed layer in the eastern tropical Pacific during the early and middle stages is not conclusive because of the large uncertainties in the estimates.

By the late stage (May 1998), SST drops in the eastern half of the basin at a much more rapid rate than can be explained by advection or surface heat flux and seems to be potentially related to the entrainment from a shallowing thermocline (the mixed depth $H$ averaged over 160°W–120°W decreases to 30–35 m from its normal value of ~50 m). Consequently, the entrainment and subthermocline mixing increase, leading to an increase of $F_w$ that results in a more rapid SST decrease because this heat loss acts on a thinner mixed layer. Note that in contrast to the early stage where SST increases were supported primarily by anomalous currents acting on a mean temperature gradient, in the middle and late stages all advective terms contribute comparably.

In summary (see Figure 7), as we found in the momentum balances, terms in the heat equation (9) become decorellated in the band of longitudes 140°W–120°W (and perhaps farther eastward). To the west, higher correlations indicate the important roles of temperature advection and surface fluxes in establishing the anomaly heat balance. To the east, lower correlations indicate the existence of other processes such as mixing at the bottom of the mixed layer and mixing by tropical instability waves [*Baturin and Niiler*, 1997]. This result is consistent with *Wang and McPhaden*'s [1999] estimates of vertical heat flux out of the base of the mixed layer.

## 4. Summary

Near-surface currents play a key role in seasonal to interannual variability in the tropical Pacific Ocean. The recent availability of extensive drogued surface drifter observations has allowed us to explore this role through direct observations. During the dramatic events of 1997–1998 we find massive changes in heat distribution and currents. Describing these changes and interpreting their impact on transports of momentum and heat as well as introducing a new data set are the goals of this study. Here we focus on the balances for three specific months: April 1997, representing the early stage; August 1997, representing the middle stage; and May 1998, representing the late stage of the 1997–1998 El Niño.

We found that during this time the linear three-term equation describes reasonably well the balance between local accel-

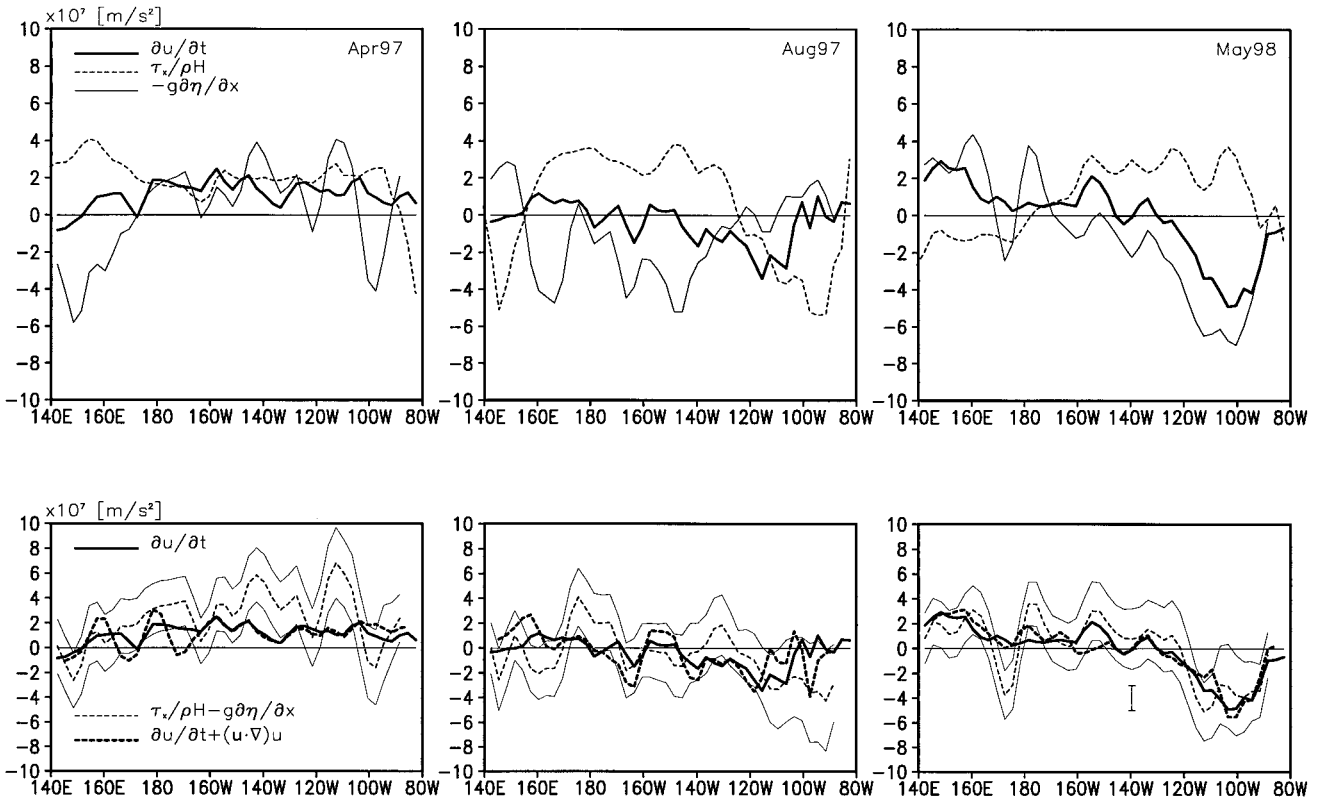


**Figure 6.** Longitudinal sections along the equator of the three terms in the linear zonal momentum balance during the early, middle, and late stages of El Niño. (top) Anomaly acceleration $\partial u/\partial t$, zonal wind stress $\tau_x/\rho H$, and pressure gradient force $-g\partial\eta/\partial x$. (bottom) Wind stress and pressure gradient terms combined, $\tau_x/\rho H - g\partial\eta/\partial x$. A vertical bar indicates standard errors for acceleration, while upper and lower thin bounding lines indicate standard errors for $\tau_x/\rho H - g\partial\eta/\partial x$. The zonal acceleration including nonlinear horizontal advection, $\partial u/\partial t + (\mathbf{u}\nabla)u$, is also shown.

eration, pressure gradient, and wind forcing. The temperature balance is nonlinear, and relative contribution of the transport terms changes in time.

Our story begins in late 1996 and early 1997 with a 1 m $s^{-1}$ eastward current anomaly equatorially trapped in the western basin, produced in response to a succession of westerly wind bursts. This current extended toward the east throughout the summer of 1997, supported by a pressure gradient force also acting in the eastward direction. The accelerating eastward currents transported the warm waters of the western warm pool east of 180°W, causing a rapid warming in mixed layer temperature as the anomalous currents acted on the mean temperature gradient, as was suggested by *Picaut et al.* [1996] and *Delcroix and Picaut* [1998]. Net surface flux was small at this time except east of 120°W, where it acted to cool the ocean as a result of increased cloudiness and latent heat loss.

By the middle stage in August the positive trade wind anomalies had extended further eastward nearly in balance with the pressure gradient force now acting to decelerate the flow. As a result, the zonal acceleration was close to zero west of 150°W. SST during this period was steady. West of 120°W, advective heat gain was balanced by surface heat loss over already warm waters. East of 120°W, surface heat loss was larger, while horizontal advection remained small. In this far eastern region, additional anomalous heat gain likely came from the anomalous deepening of the thermocline by 25 m and the consequent reduction in cooling due to mixing and transport across the base of this layer.

By the later stage in May 1998 the positive trade wind anomalies shifted far to the east. However, an intense negative pressure gradient force caused a strong westward acceleration. SST decreased rapidly in the eastern half of the basin. This decrease was larger than could be balanced by advection or surface heat flux and seems clearly to have been related to the loss of heat associated with the entrainment from a shallowing thermocline (which rose by 25 m between 160°W and 120°W).

Our results show the interplay in the mixed layer temperature budget between advection, surface fluxes, and diagnosed vertical heat flux out of the base of the mixed layer. The relative importance of each term varies along the equator and in time as the 1997–1998 El Niño progresses.

The robustness of our conclusions depends on the accuracy of the surface velocity analysis. The authors foresee improvement of this analysis through the use of additional information such as historical ship drifts, TAO buoy currents, and ADCP measurements.

## Appendix A

After some algebra [see *Daley*, 1981, p. 164] the covariance functions take the form

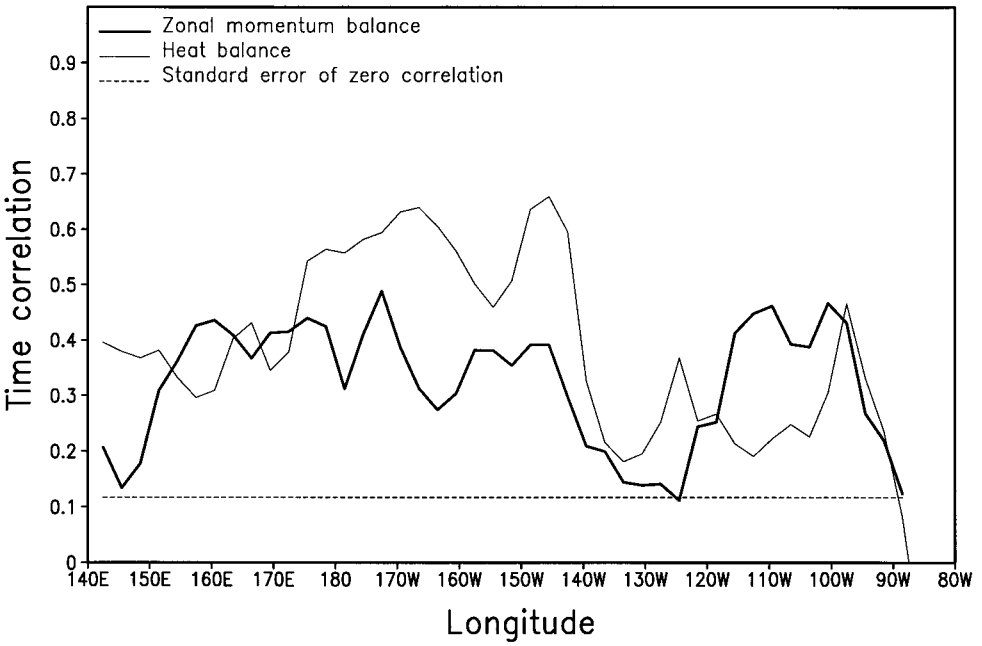


**Figure 7.** Longitudinal sections along the equator of the correlation over time of the left- and right-hand sides in the zonal momentum (equation (8)) and heat budget (equation (9)) equations. The correlation between zonal acceleration and the difference between anomaly zonal wind stress and anomaly zonal pressure gradient is denoted by a thick line, while the correlation between SST rate of change and the difference between net heat flux and temperature advection is denoted by a thin line.

$$\mathrm{Cov}\,(u_r,\,\eta_p) = \frac{2g}{r_y^2}\left[-W(\varphi_r)\,\frac{\Delta y}{f_r} + \frac{1-W(\varphi_r)}{\beta}\left(1-\frac{2\Delta y^2}{r_y^2}\right)\right]\mathrm{Cov}\,(\eta_r,\,\eta_p), \tag{A1}$$

$$\mathrm{Cov}\,(v_r,\,\eta_p) = \frac{2g}{r_x^2}\,W(\varphi_r)\,\frac{\Delta x}{f_r}\,\mathrm{Cov}\,(\eta_r,\,\eta_p), \tag{A2}$$

$$\begin{aligned}\mathrm{Cov}\,(u_r,\,u_s) = {} & \frac{4g^2(1-W(\varphi_r))(1-W(\varphi_s))}{\beta^2 r_y^4}\\ & \cdot\left[2+\left(1-\frac{2\Delta y^2}{r_y^2}\right)^2\right]\mathrm{Cov}\,(\eta_r,\,\eta_s) + \frac{4g^2\Delta y}{\beta r_y^4}\\ & \cdot\left[[1-W(\varphi_r)]\,\frac{W(\varphi_s)}{f_s} - [1-W(\varphi_s)]\,\frac{W(\varphi_r)}{f_r}\right]\\ & \cdot\left(3-\frac{2\Delta y^2}{r_y^2}\right)\mathrm{Cov}\,(\eta_r,\,\eta_s) + \frac{2g^2}{r_y^2}\,\frac{W(\varphi_s)}{f_s}\,\frac{W(\varphi_r)}{f_r}\\ & \cdot\left(1-\frac{2\Delta y^2}{r_y^2}\right)\mathrm{Cov}\,(\eta_r,\,\eta_s),\end{aligned} \tag{A3}$$

$$\begin{aligned}\mathrm{Cov}\,(u_r,\,v_s) = {} & -\frac{4g^2(1-W(\varphi_r))W(\varphi_s)\Delta x}{\beta f_s r_x^2 r_y^2}\\ & \cdot\left(1-\frac{2\Delta y^2}{r_y^2}\right)\mathrm{Cov}\,(\eta_r,\,\eta_s)\\ & + \frac{4g^2 W(\varphi_r)W(\varphi_s)\Delta x\Delta y}{f f_s r_x^2 r_y^2}\,\mathrm{Cov}\,(\eta_r,\,\eta_s),\end{aligned} \tag{A4}$$

$$\mathrm{Cov}\,(v_r,\,v_s) = \frac{2g^2}{r_x^2}\,\frac{W(\varphi_s)}{f_s}\,\frac{W(\varphi_r)}{f_r}\left(1-\frac{2\Delta x^2}{r_x^2}\right)\mathrm{Cov}\,(\eta_r,\,\eta_s). \tag{A5}$$

## Appendix B: Error Estimates

Let $\varepsilon(x)$ denote the standard error of any variable $x$. Our estimate of the accuracy of the velocity analysis is based on a posteriori comparison with TAO mooring measurements. Here we accept that $\varepsilon(u) = 0.3$ m s$^{-1}$ and $\varepsilon(v) = 0.1$ m s$^{-1}$ are equal to typical values of standard deviation between analysis current and buoy data. Thus the error of the acceleration term is $\varepsilon(\partial u/\partial t) = \sqrt{2}\varepsilon(u)/\Delta t \approx 10^{-7}$ m s$^{-2}$ for central differences taken at $\Delta t = 2$ months. If we assume the sea level error $\varepsilon(\eta) = 2$ cm for $1^\circ \times 1^\circ \times 1$ month binned data (following *Cheney et al.* [1994]) and add a smoothing factor $n = 6$ for data averaged into a $2^\circ \times 3^\circ \times 1$ month grid (accounting for independent measurement errors at different locations), then the standard error of the sea level slope becomes $\varepsilon(g\partial\eta/\partial x) = g\sqrt{2/n}\varepsilon(\eta)/\Delta x \approx 2 \times 10^{-7}$ m s$^{-2}$. The wind stress error ($\varepsilon(\tau_x)$) dependence on wind speed error ($\varepsilon(U)$) follows from a simple bulk formula based on a drag coefficient $C_D$ and equals $\varepsilon(\tau_x) = 2\sqrt{C_D\rho_a/\tau}|\tau_x|\varepsilon(U)$. To estimate $\varepsilon(\tau_x)$, we accept $\varepsilon(U) = 1$ m s$^{-1}$ and $C_D = 1.4 \times 10^{-3}$.

Error estimates in the temperature equations follow similar reasoning. We assume that the SST observations are subject to a random error of $\varepsilon(T) = 0.1$°C. This estimate follows from a maximum value of 0.4°C for deviation from in situ data of the $1^\circ \times 1^\circ$ weekly SST analysis by *Reynolds and Smith* [1994] and a factor of $1/24^{0.5}$ accounting for monthly averaging and $2^\circ \times 3^\circ$ smoothing. Thus the standard error is $\varepsilon(\partial T/\partial t) = \sqrt{2}\varepsilon(T)/\Delta t = 0.3 \times 10^{-7}$°C s$^{-1}$. Errors in the advection term derive primarily from errors in velocity $\varepsilon(Q_u) =$

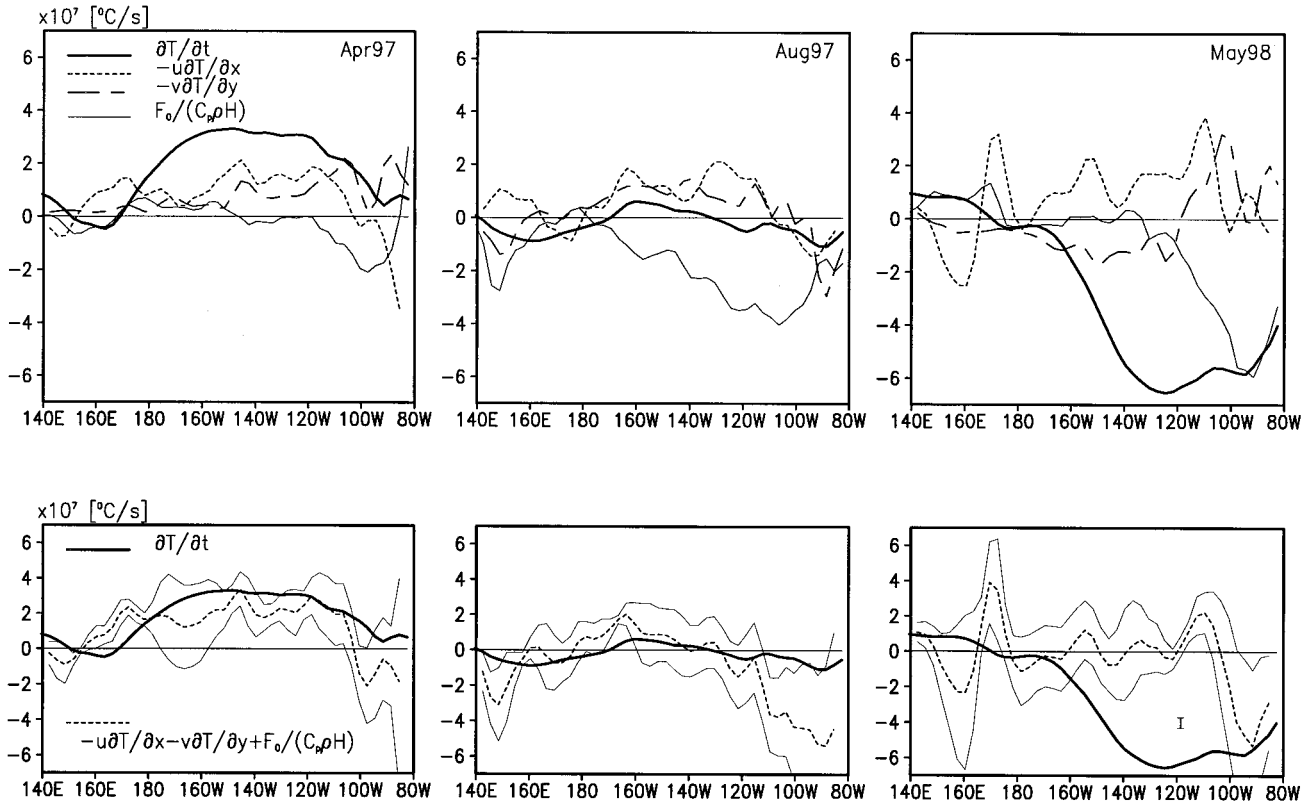


**Figure 8.** Longitudinal sections along the equator of the terms in the heat budget equation (equation (9)) during the same three months as in Figure 6. (top) Rate of change of SST ($\partial T/\partial t$), zonal ($-u\partial T/\partial x$) and meridional ($-v\partial T/\partial y$) advection, and effective surface heat flux ($F_0/C_p\rho H$). (bottom) Heat advection and heat flux terms combined. A vertical bar indicates standard errors for the SST rate of change, while upper and lower thin bounding lines indicate standard errors for the term combining the effects of advection and surface heat flux. Note that an SST rate of change of $10^{-7}$°C s$^{-1}$ corresponds to heat flux of 28 and 10 W m$^{-2}$ for the mixed layer thickness of $H = 70$ m and $H = 25$ m, respectively, typical of the central and eastern parts of the basin.

$\sqrt{\varepsilon^2(u)(\partial T/\partial x)^2 + \varepsilon^2(v)(\partial T/\partial y)^2}$, where $\varepsilon^2(u) = 0.1$ m$^2$ s$^{-2}$, and $\varepsilon^2(v) = 0.01$ m$^2$ s$^{-2}$. Finally, we accept the optimistic $\varepsilon(Q_0) = 5$ W m$^{-2}$ error estimate of *Kistler et al.* [2001] for the surface flux data.

**Acknowledgments.** This work has been supported by the National Science Foundation (OCE9530220 and OCE9812404). We gratefully acknowledge Mark Swenson, formerly of the NOAA Atlantic Oceanographic Marine Laboratory, for providing the surface drifter data set. Chet Koblinsky of NASA Goddard Space Flight Center provided the altimeter data. We are grateful to Eric Johnson of Earth and Space Research and to an anonymous reviewer for valuable comments.

## References

Acero-Schertzer, C. E., D. V. Hansen, and M. S. Swenson, Evaluation and diagnosis of surface currents in the National Center for Environmental Prediction's ocean analyses, *J. Geophys. Res.*, *102*, 21,037–21,048, 1997.

An, S.-I., F.-F. Jin, and I.-S. Kang, The role of zonal advection feedback in phase transition and growth of ENSO in the Cane-Zebiak model, *J. Meteorol. Soc. Jpn.*, *77*, 1151–1160, 1999.

Baturin, N. G., and P. P. Niiler, Effects of instability waves in the mixed layer of the equatorial Pacific, *J. Geophys. Res.*, *102*, 27,771–27,793, 1997.

Carton, J. A., and E. C. Hackert, Application of multivariate statistical objective analysis to the circulation in the tropical Atlantic Ocean, *Dyn. Atmos. Oceans*, *13*, 491–515, 1989.

Carton, J. A., B. S. Giese, X. Cao, and L. Miller, Impact of altimeter, thermistor, and expendable bathythermograph data on retrospective analyses of the tropical Pacific Ocean, *J. Geophys. Res.*, *101*, 14,147–14,159, 1996.

Carton, J. A., G. Chepurin, X. Cao, and B. Giese, A simple ocean data assimilation analysis of the global upper ocean 1959–1995, part 1, Methodology, *J. Phys. Oceanogr.*, *30*, 294–309, 2000.

Cheney, R., L. Miller, R. Agreen, N. Doyle, and J. Lillibridge, TOPEX/Poseidon: The 2-cm solution, *J. Geophys. Res.*, *99*, 24,555–24,563, 1994.

Daley, R., *Atmospheric Data Analysis*, 457 pp., Cambridge Univ. Press, New York, 1991.

Delcroix, T., and J. Picaut, Zonal displacement of the western equatorial Pacific "fresh pool," *J. Geophys. Res.*, *103*, 1087–1098, 1998.

DeWitt, D. G., and E. K. Schneider, The processes determining the annual cycle of equatorial sea surface temperature: A coupled general circulation model perspective, *Mon. Weather Rev.*, *127*, 381–395, 1999.

Hansen, D. V., and P.-M. Poulain, Quality control and interpolations of WOCE-TOGA drifter data, *J. Atmos. Oceanic Technol.*, *13*, 900–909, 1996.

Jin, F.-F., and S.-I. An, Thermocline and zonal advective feedbacks within the equatorial ocean recharge oscillator model for ENSO, *Geophys. Res. Lett.*, *26*, 2989–2992, 1999.

Johnson, E. S., and D. S. Luther, Mean zonal momentum balance in the upper and central equatorial Pacific Ocean, *J. Geophys. Res.*, *99*, 7689–7705, 1994.

Johnson, G. C., M. J. McPhaden, G. D. Rowe, and K. E. McTaggart, Upper equatorial Pacific Ocean current and salinity variability during the 1996–1998 El Niño–La Niña cycle, *J. Geophys. Res.*, *105*, 1037–1053, 2000.

Johnston, T. M. S., and M. A. Merrifield, Interannual geostrophic

current anomalies in the near-equatorial western Pacific, *J. Phys. Oceanogr*., *30*, 3–14, 2000.
Kalnay, E., et al., The NCEP/NCAR 40-year reanalysis project, *Bull. Am. Meteorol. Soc*., *77*, 437–471, 1996.
Kessler, W. C., L. M. Rothstein, and D. Chen, The annual cycle of SST in the eastern tropical Pacific, diagnosed in an ocean GCM, *J. Clim*., *11*, 777–799, 1998.
Kistler, R., et al., The NCEP/NCAR 50-year reanalysis: Monthly means CD-ROM and documentation, *Bull. Am. Meteorol. Soc*., *82*, 247–268, 2001.
Köberle, C., and S. G. H. Philander, On the processes that control seasonal variations of sea surface temperatures in the tropical Pacific Ocean, *Tellus*, *Ser. A*, *46*, 481–496, 1994.
Koblinsky, C. J., B. D. Beckley, S. Howden, L. Tsaoussi, L. Wang, and Y. M. Wang, Sea surface topography over the past decade observed from satellite altimeters, paper presented at International Symposium, TOPEX/Poseidon Sci. Working Team Meet., Biarritz, France, Oct. 13–17, 1997.
Lagerloef, G. S. E., G. T. Mitchum, R. B. Lukas, and P. P. Niiler, Tropical Pacific near-surface currents estimated from altimeter, wind, and drifter data, *J. Geophys. Res*., *104*, 23,313–23,326, 1999.
McPhaden, M. J., Genesis and evolution of the 1997–1998 El Niño, *Science*, *283*, 950–954, 1999.
McPhaden, M. J., et al., The Tropical Ocean–Global Atmosphere observing system: A decade of progress, *J. Geophys. Res*., *103*, 14,169–14,240, 1998.
Menkes, C., J.-P. Boulanger, and A. J. Busalacchi, Evaluation of TOPEX and basin-wide Tropical Ocean and Global Atmosphere–Tropical Atmosphere-Ocean sea surface topographies and derived geostrophic currents, *J. Geophys. Res*., *100*, 25,087–25,099, 1995.
Moisan, J. R., and P. P. Niiler, The seasonal heat budget of the North Pacific: Net heat flux and heat storage rates (1950–1990), *J. Phys. Oceanogr*., *28*, 401–421, 1998.
Niiler, P. P., R. E. Davis, and H. J. White, Water-following characteristics of a mixed layer drifter, *Deep Sea Res*., *Part A*, *34*, 1867–1882, 1987.
Picaut, J., S. P. Hayes, and M. J. McPhaden, Use of geostrophic approximation to estimate time-varying zonal currents at the equator, *J. Geophys. Res*., *94*, 3228–3236, 1989.
Picaut, J., M. Ioualalen, C. Menkes, T. Delcroix, and M. J. McPhaden, Mechanism of the zonal displacements of the Pacific warm pool: Implications for ENSO, *Science*, *274*, 1486–1489, 1996.
Picaut, J., F. Masia, and Y. du Penhoat, An advective-reflective conceptual model for the oscillatory nature of the ENSO, *Science*, *277*, 663–666, 1997.
Qiao, L., and R. H. Weisberg, The zonal momentum balance of the equatorial undercurrent in the central Pacific, *J. Phys. Oceanogr*., *27*, 1094–1119, 1997.
Ralph, E. A., and P. P. Niiler, Wind-driven currents in the tropical Pacific, *J. Phys. Oceanogr*., *29*, 2121–2129, 1999.
Reynolds, R. W., and T. M. Smith, Improved global sea surface temperature analyses using optimum interpolation, *J. Clim*., *7*, 929–948, 1994.
Suarez, M. J., and P. S. Schopf, A delayed action oscillator for ENSO, *J. Atmos. Sci*., *45*, 3283–3287, 1988.
Swenson, M. S., and D. V. Hansen, Tropical Pacific Ocean mixed layer heat budget: The Pacific cold tongue, *J. Phys. Oceanogr*., *29*, 69–81, 1999.
Wang, C. Z., and R. H. Weisberg, The 1997–98 El Niño evolution relative to previous El Niño events, *J. Clim*., *13*, 488–501, 2000.
Wang, W. M., and M. J. McPhaden, The surface-layer heat balance in the equatorial Pacific Ocean, part I, Mean seasonal cycle, *J. Phys. Oceanogr*., *29*, 1812–1831, 1999.
Wyrtki, K., Water displacements in the Pacific and genesis of El Niño cycles, *J. Geophys. Res*., *90*, 7129–7132, 1985.
Yu, X. R., and M. J. McPhaden, Dynamical analysis of seasonal and interannual variability in the equatorial Pacific, *J. Phys. Oceanogr*., *29*, 2350–2369, 1999.
Yu, L. A., and M. M. Rienecker, Evidence of an extratropical atmospheric influence during the onset of the 1997–1998 El Niño, *Geophys. Res. Lett*., *25*, 3537–3540, 1998.
Yu, Y., W. J. Emery, and R. R. Leben, Satellite altimeter derived geostrophic currents in the western tropical Pacific during 1992–1993 and their validation with drifting buoy trajectories, *J. Geophys. Res*., *100*, 25,069–25,085, 1995.

J. A. Carton and S. A. Grodsky, Department of Meteorology, University of Maryland, 2417 Computer and Space Sciences Building, College Park, MD 20742. (carton@metosrv2.umd.edu; senya@ocean2.umd.edu)

(Received June 8, 2000; revised February 9, 2001;
accepted March 13, 2001.)